

# Atmospheric properties and the ENSO cycle: models versus observations

Sjoukje Y. Philip · Geert Jan van Oldenborgh

Received: date / Accepted: date

**Abstract** Two important atmospheric features affecting the ENSO cycle are weather noise and a nonlinear atmospheric response to SST. In this article we investigate the roles of these atmospheric features in ENSO in observations and coupled Global Climate Models (GCMs).

We first quantify the most important linear couplings between the ocean and atmosphere. We then characterize atmospheric noise by its patterns of standard deviation and skewness and by spatial and temporal correlations. GCMs tend to simulate lower noise amplitudes than observations. Additionally we investigate the strength of a nonlinear response of wind stress to SST. Some GCMs are able to simulate a nonlinear response of wind stress to SST, although weaker than in observations. These models simulate the most realistic SST skewness.

The influence of the couplings and noise terms on the ENSO cycle are studied with an Intermediate Climate Model (ICM). With couplings and noise terms fitted to either observations or GCM output, the simulated climates of the ICM versions show differences in the ENSO cycle similar to differences in ENSO characteristics in the original data. In these model versions the skewness of noise is of minor influence on the ENSO cycle than the standard deviation of noise. Both the nonlinear response of wind stress to SST anomalies and the relation of noise to the background SST contribute to SST skewness.

Overall, atmospheric noise with realistic standard deviation pattern and spatial correlations seems to be important for simulating an irregular ENSO cycle. Both a nonlinear at-

mospheric response to SST and the dependence of noise on the background SST influence the El Niño/La Niña asymmetry.

**Keywords** ENSO · stochastic forcing · nonlinearities · climate models · validation

## 1 Introduction

The El Niño – Southern Oscillation (ENSO) is one of the most important climate modes on interannual time scales. This climate phenomenon has been extensively studied in both observations and models. The basic linear physics of the ENSO cycle is well understood, but more work is required on the physical mechanisms determining irregularities and asymmetries, e.g., El Niño events are in general larger than La Niña events. For example, two candidate mechanisms for asymmetries and irregularities in the ENSO cycle that have been proposed are nonlinear internal dynamics and stochastic forcing.

Different types of nonlinear internal dynamics have been studied. Jin et al (2003) claim that nonlinear dynamical heating is an important nonlinearity in the eastern Pacific. In the Cane-Zebiak model of ENSO (Zebiak and Cane 1987) a nonlinear coupling exists between sea surface temperature (SST) and the thermocline depth. Furthermore, the wind stress response to SST anomalies is not linear everywhere, and noise components in the wind that drive anomalies in the ocean can depend strongly on the background SST, like in the model of Kleeman et al (1995). Nonlinear analysis methods such as nonlinear principal component analysis have been used (e.g., An et al 2005) to show that ENSO is a nonlinear cyclic phenomenon.

The role of atmospheric stochastic forcing has also been studied extensively. Blanke et al (1997) suggested that the addition of atmospheric noise increases ENSO irregularity

---

S.Y. Philip  
KNMI, De Bilt, The Netherlands  
Tel.: +31-(0)30-2206704  
E-mail: philip@knmi.nl

G.J. van Oldenborgh  
KNMI, De Bilt, The Netherlands

and that the ocean is sensitive to the spatial coherence of noise fields. More recent studies focus on the interaction between ENSO and the atmospheric variability at shorter timescales such as the Madden-Julian Oscillation (MJO), and westerly wind events (WWEs) in both observations (e.g. Lengaigne et al 2003; Vecchi et al 2006; Kug et al 2008a) and coupled models (e.g. Lengaigne et al 2004). Some studies prescribe noise with an idealized structure in models (Eisenman et al 2005; Gebbie et al 2007; Tziperman and Yu 2007), others use Principal Component Analysis (Zavala-Garay et al 2003; Perez et al 2005; Zhang et al 2008).

The latest generation of coupled climate models can produce a climate in which ENSO-like behavior is present, but improvements could still be made. Most climate models still do not capture for instance SST skewness: the fact that La Niña events occur more frequently but are weaker than El Niño events, see also Figure 10. Among the current generation of models even the most reliable coupled models show large differences (e.g., van Oldenborgh et al 2005; Guilyardi 2006). It is an open question to what extent linear or nonlinear feedbacks or noise terms are responsible for these differences.

Philip and van Oldenborgh (2008) show that the nonlinear response of wind stress to SST anomalies largely influences the ENSO cycle in terms of SST skewness. Furthermore, the noise terms, defined as the wind stress residual of a (nonlinear) statistical atmosphere model, are described in terms of standard deviation, skewness, spatial correlations and temporal correlations. These noise terms do depend on the background SST. With an Intermediate Climate Model (ICM) for the Pacific Ocean in which feedbacks and noise terms are fitted to weekly observations this study shows that the spatial coherent field of noise in terms of standard deviation strongly influences SST variability. The noise skewness has only a minor influence. Furthermore, the nonlinear response of wind stress to SST anomalies affects SST skewness most, followed by the dependence of the noise standard deviation pattern on the background state.

As coupled global climate models (GCMs) still show large discrepancies with the observed ENSO cycle we investigate the differences in these modeled processes and atmospheric noise terms compared to the observed ones as described in Philip and van Oldenborgh (2008). This study examines a selection of five coupled GCMs that most realistically simulate ENSO properties and linear feedbacks in the ENSO cycle, (see also van Oldenborgh et al (2005) and Section 2.3). We build linear, coupled ICM versions of these GCMs so that the dynamics are much easier to understand. With these ICM versions we are able to study the influence of additional noise properties or nonlinear terms on the characteristics of the ENSO cycle.

The question addressed in this paper is: what are the most important similarities and dissimilarities in atmospheric

properties between observations and GCMs influencing the ENSO cycle?

This question is answered in two steps, the methodology of which will be explained in detail in Section 2. In Section 3 we directly compare atmospheric noise terms of GCMs with atmospheric noise terms of observations. Section 4 compares nonlinearities in the description of the atmosphere of observations with GCMs. The influence of noise and nonlinear terms on the ENSO cycle is described in Section 5. Finally, conclusions are drawn in Section 6.

## 2 Method of investigation

We use the framework sketched in Figure 1 to describe the ENSO cycle. In this simplified model coupling strengths are fitted from observations and five GCMs. The atmospheric response to equatorial SST anomalies is described by a statistical atmosphere model. Here, we consider the atmospheric component that is dynamically most important, the zonal wind stress ( $\tau_x$ ) (Philander 1990). Heat fluxes play a role as well, but are implemented as a damping term in the SST equation. A nonlinear atmospheric response is described with a second order term in the statistical atmosphere model. The noise is defined as the residual of the observed or GCM modeled wind stress minus the quantity described by the (nonlinear) statistical atmosphere. This noise is described by the first two non-zero statistical moments: standard deviation and skewness. This description does not include a dynamical structure in the noise terms. However, the ocean acts as a low pass filter. When the ocean model used in this study (see later) is forced with observed wind stress it shows similar SST characteristics compared to when the model is forced with noise characterized as above.

The other main couplings between zonal wind stress, SST and thermocline depth ( $Z_{20}$ ) are fitted separately. The resulting set of coupling strengths describes all interactions in the conceptual ENSO model shown in Figure 1. Figure 1a shows the linear approximation, Figure 1b describes the nonlinear components that have been included in this study: the internal nonlinear response of wind stress to SST and the external noise terms.

In the next subsections we first describe how the coupling strengths and noise parameters were estimated. Then we explain how these were used to infer the influence of the atmospheric properties on the ENSO cycle.

### 2.1 Fitting the couplings and noise of the ENSO cycle

To start with, all linear and nonlinear couplings between  $\tau_x$ , SST and  $Z_{20}$  and atmospheric noise terms as shown in Figure 1 are separately fitted to observations and GCM output. The linear feedbacks include a linear statistical atmosphere

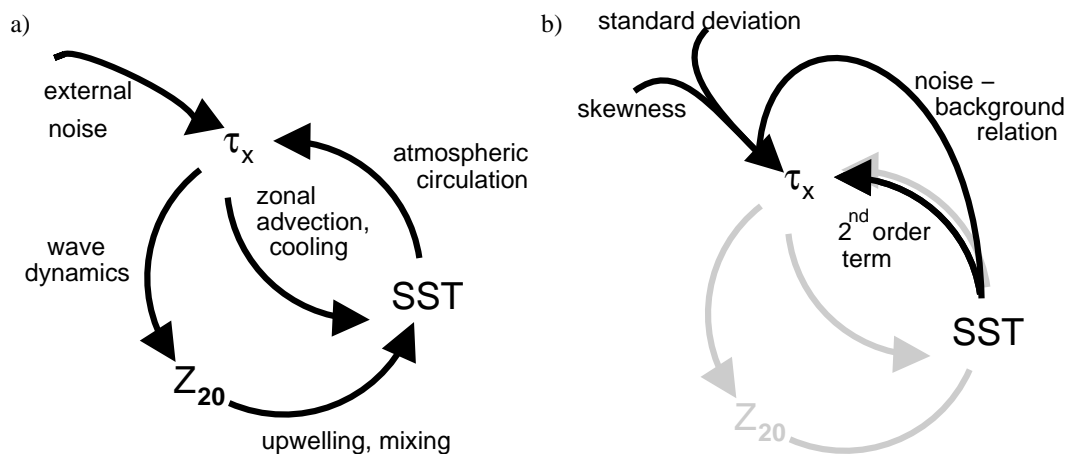


**Fig. 1** The main feedbacks between wind stress ( $\tau_x$ ), SST and thermocline depth ( $Z_{20}$ ) in the ENSO cycle and the external noise term. a) linear feedbacks and b) the contribution of noise properties and nonlinear terms examined in this study.

and a linear SST anomaly equation (investigated by van Oldenborgh et al (2005)) and a Kelvin wave speed. In this paper we extend the study with a description of the noise terms. Furthermore the characteristics of couplings fitted to GCMs will be compared in some more detail with the characteristics of the fitted couplings of observations.

The noise terms of both observations and GCMs are characterized by two-dimensional standard deviation and skewness patterns and spatial and temporal correlation. In addition to the linear feedbacks the nonlinear, second order response of wind stress to SST is investigated. Subsequently, the relation between noise and the background SST is characterized. (The exact method of fitting the couplings and noise terms with governing equations will be described in Sections 3 and 4.)

Once all components of the conceptual model are characterized for both observations and different GCMs, the terms of GCMs are compared to the observed characteristics. This shows to what extent the atmospheric noise and the nonlinear response of wind stress to SST anomalies of models correspond with the observed characteristics.

## 2.2 Influence of couplings and noise on the ENSO cycle

The influence of atmospheric noise and the nonlinear wind stress response to SST on the ENSO cycle is studied with an Intermediate Complexity Model (ICM). This ICM is based on the so called Gmodel (Burgers et al 2002; Burgers and van Oldenborgh 2003). The extended version of the Gmodel uses a more comprehensive conceptual model of ENSO than the original one (Figure 1b).

For a selection of five GCMs and for observations (see Section 2.3) the fitted components are coupled together, resulting in six versions of the extended Gmodel.

Apart from the statistical atmosphere and SST equation, the extended Gmodel consists of a linear 1.5-layer reduced-gravity ocean model. It solves the shallow water equations (Gill 1982). The model domain ranges from  $30^{\circ}\text{S}$  to  $30^{\circ}\text{N}$  and  $122^{\circ}\text{E}$  to  $292^{\circ}\text{E}$ , on a  $2^{\circ} \times 1^{\circ}$  longitude-latitude grid with realistic coast lines. The ICM is driven by wind stress noise obtained from the statistical atmosphere model.

Simulations are performed with these six versions of the extended Gmodel. Nonlinearities and noise characteristics are added one by one. Using these tuned reduced models we estimate the influence of the similarities and dissimilarities of atmospheric noise and the nonlinear response of wind stress to SST described in Section 2.1.

## 2.3 Data

Observations (OBS) are approximated by two reanalysis datasets. For the statistical atmosphere and the noise terms, monthly ERA-40 data (Uppala et al 2005) have been used. The ocean parameters are fitted to the monthly SODA 1.4.2/3  $0.5^{\circ}$  ocean reanalysis dataset (Carton and Giese 2008).

The set of GCMs we use in this study is a selection of five climate models that were available in the CMIP3-archive. The selection consists of GFDL\_CM2.0 (GFDL2.0), GFDL\_CM2.1 (GFDL2.1), ECHAM5/MPI-OM (ECHAM5), MIROC3\_2(medres) (MIROC) and UKMO-HadCM3 (HadCM3). These models were found to have the most realistic description of the linear feedbacks defined in Figure 1a (van Oldenborgh et al 2005).

## 3 Noise properties and coupling strengths

The main components in the conceptual model (Figure 1) are: a statistical atmosphere model, atmospheric noise prop-

erties, an ocean model and an SST equation. Each of them will be fitted and discussed separately in the next four subsections.

### 3.1 Statistical atmosphere model

The atmosphere is described by a statistical atmosphere model with as basis for SST  $n$  equal-sized boxes along the equator in  $5^\circ\text{S}$ – $5^\circ\text{N}$ ,  $140^\circ\text{E}$ – $80^\circ\text{W}$ . Zonal wind stress anomalies are described with a linear statistical atmosphere model as a direct response to SST anomalies (e.g. Von Storch and Zwiers 2001, §8.3):

$$\tau'_x(x, y, t) = \sum_{i=1}^n A_{1,i}(x, y) T'_i(t) + \varepsilon_1(x, y, t) \quad (1)$$

where  $\tau'_x(x, y, t)$  is the domain-wide zonal wind stress anomaly and  $T'_i(t)$  are SST anomalies averaged over separate regions  $i = 1, 2, \dots, n$ . The patterns  $A_{1,i}(x, y)$  are the domain-wide wind stress patterns corresponding to these SST anomalies. The term  $\varepsilon_1(x, y, t)$  denotes the stochastic forcing by random wind stress variations. A next section is devoted to the properties of this noise term. The subscript 1 refers to the linear model (see later).

The wind stress patterns of ERA-40 resemble a Gill response (Gill 1980): for  $n = 3$ , the linear wind response to a positive SST anomaly in the central box is directed eastward in the West Pacific and westward in the East Pacific. Details such as the relative strengths of the equatorial responses and the off-equatorial structure differ from the Gill-type pattern. In the five GCMs the strength of the  $\tau_x$  response to SST anomalies is in general weaker and the off-equatorial structures differ. A detailed description of all wind stress patterns is given by van Oldenborgh et al (2005).

With this description of the atmosphere the three wind stress patterns correspond to an SST anomaly in one of these three boxes only, and they are insensitive to the SST anomalies in the other two boxes. In the GCM data, a zonal shift of the boxes would result in a zonal shift of the patterns  $A_{1,i}(x, y)$ . Curiously, this is not the case in the ERA-40 data, where for any index region the pattern always resembles a linear combination of the responses to the Niño3 and Niño4 indices. As it is unclear whether this is a model error or a lack of observational data we use the same three boxes as defined above throughout.

### 3.2 Noise properties of wind stress

In Eq. 1, the noise  $\varepsilon_1(x, y, t)$  is defined as the part of the wind stress anomaly that is not described by the statistical atmosphere model. From Blanke et al (1997) we learn that noise amplitude and spatial coherence influence the ENSO cycle. Burgers and van Oldenborgh (2003) show that the

time-correlation also strongly influences the amplitude of ENSO. The skewed nature of the zonal wind stress may have an effect on the ENSO skewness. Therefore the time-dependent noise fields are parameterized by the following statistical properties: standard deviation  $\sigma(x, y)$ , skewness  $S(x, y)$ , spatial correlation lengths  $a_x(x, y)$  and  $a_y(x, y)$  and temporal correlation  $a_1(x, y)$ .

For the ERA-40 reanalysis the noise the standard deviation is shown in Figure 2 (left panels). Near the equator the noise standard deviation is highest in the West Pacific where temperatures are highest. The variance of the noise increases with latitude.

This structure is well captured by the five GCMs, but in general with a much lower amplitude on the equator and a higher amplitude off the equator (Figure 2). Compared to ERA-40, the standard deviation of the noise in the GFDL2.1 model is only 20% lower near the equator, and 40% stronger at higher latitudes. However, for GFDL2.0 and ECHAM5 the standard deviation is almost 40% lower near the equator and stronger at higher latitudes, 40% and 20% respectively. In the HadCM3 model the noise amplitude most notably differs from ERA-40 near the equator, with an underestimation of 40%. Finally, the atmospheric component of the MIROC model generates the least variability in zonal wind stress at the equator, with a standard deviation that is more than two times lower at the equator than that of ERA-40.

The skewness of the ERA-40 noise is shown in Figure 2 (right panels). In the warmer West Pacific strong, short time scale WVEs occur frequently. These cause the distribution of zonal wind stress to be positively skewed. The skewness reaches values up to 1.0 in this area. The GFDL2.0 model is very similar to ERA-40. Also, the noise of both the GFDL2.1 and ECHAM5 models is positively skewed in the West Pacific, although too strongly. The HadCM3 and MIROC models do not generate significant skewness in the noise. The latter two models therefore do not generate features which resemble the observed WVEs.

The spatial and lag one time-correlations are estimated at 25 equally distributed locations between  $30^\circ\text{S}$ – $30^\circ\text{N}$ ,  $122^\circ\text{E}$ – $272^\circ\text{E}$ , that is, 5 locations zonally times 5 locations meridionally, capturing the main features in the entire basin. For ERA-40 the spatial correlation length varies very little from 36 degrees in longitude ( $a_x$ ) and varies between 6 (between  $10^\circ\text{N}$  and  $10^\circ\text{S}$ ) and 8 (higher latitudes) degrees in latitude ( $a_y(y)$ ). For the GCMs the spatial correlation is slightly lower:  $a_x = 24$  (20 for ECHAM5) and  $a_y = 4$ .

A good approximation of the time-correlation coefficient at lag one month  $a_1(x, y)$  is given by a function that varies linearly along the equator and exponentially along the meridionals as

$$a_1(x, y) = 0.55 \frac{1 - (x - x_W)}{16(x_E - x_W)} e^{-|y|/12} \quad (2)$$

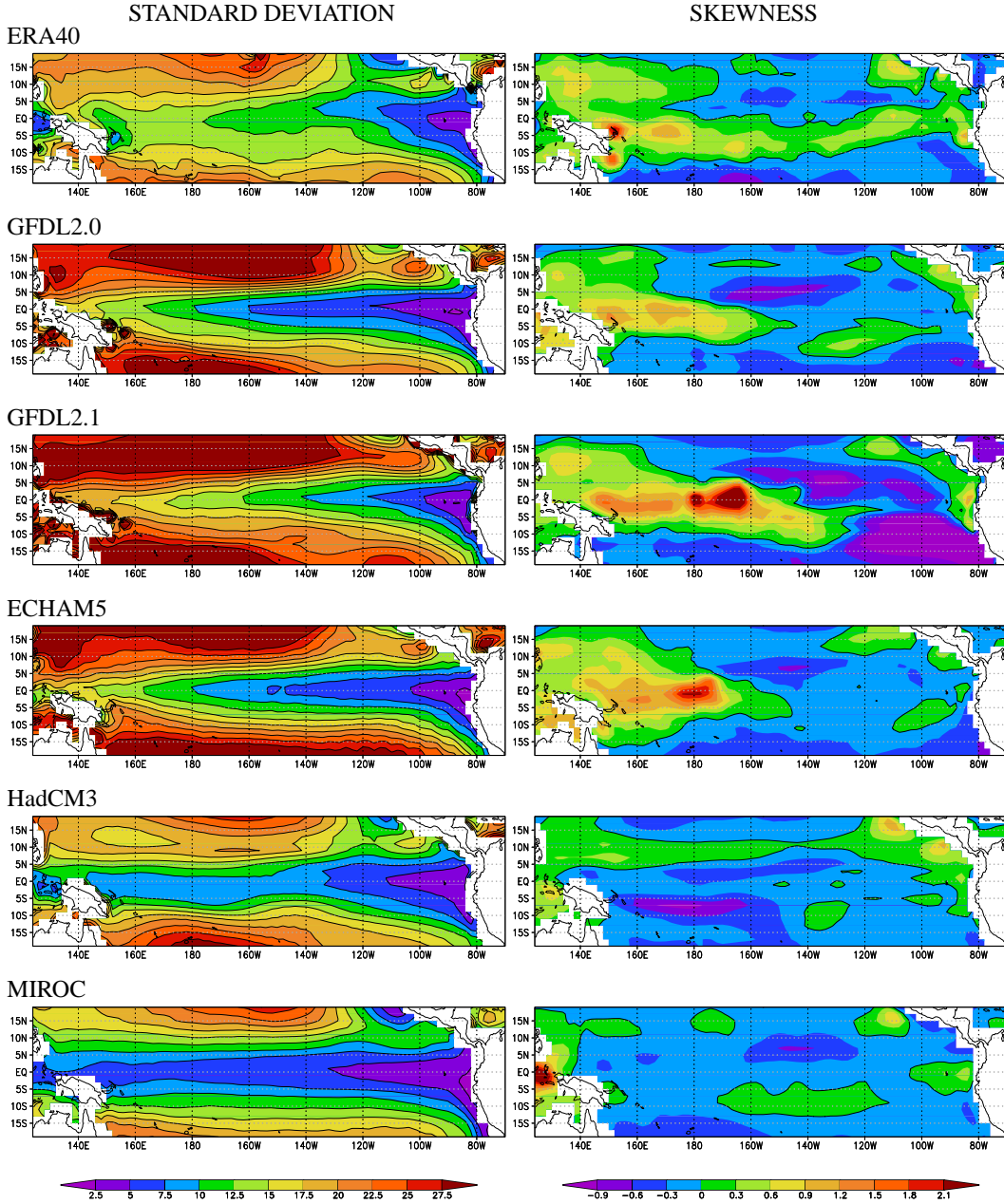


**Fig. 2** Standard deviation [ $10^{-3}\text{Nm}^{-2}$ ] (left) and skewness (right) of atmospheric noise. The top panels show noise characteristics for ERA-40 reanalysis data, the other panels show the characteristics of noise of GCM data.

with  $x, y$  ranging between the boundaries of the domain  $x_E, x_W, y_S$  and  $y_N$ . This gives correlations around 0.45 near the equator and 0.1 near the northern and southern edges of the domain. The average autocorrelation of zonal wind stress averaged over the Niño34 region ( $5^\circ\text{S}: 5^\circ\text{N}, 190^\circ\text{E}: 240^\circ\text{E}$ ) is shown in Figure 3.

The temporal correlations of zonal wind stress noise in the GFDL2.0, GFDL2.1 and HadCM3 models are comparable to that of ERA-40. In the ECHAM5 and MIROC models the temporal correlation is almost zero.

### 3.3 Reduced gravity shallow water model

The response of thermocline anomalies  $Z'_{20}$  to zonal wind stress anomalies  $\tau'_x(x, y, t)$  (see Figure 1a) is captured by the shallow water equations. The one free parameter of the reduced gravity ocean model that is used solve these equations is the Kelvin wave speed (Burgers et al 2002). This Kelvin wave speed is fitted to optimize ocean dynamics in the six un-coupled versions of the extended Gmodel. Values range between  $1.9 \text{ ms}^{-1}$  for HadCM3 to  $2.5 \text{ ms}^{-1}$  in the observations (see Table 1). All the models show a lower Kelvin

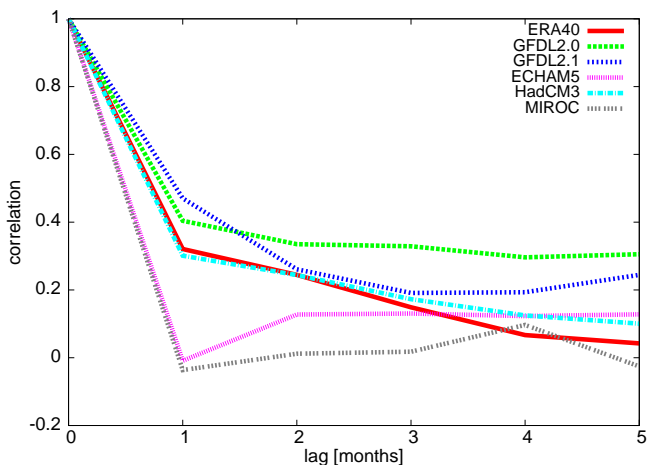


**Fig. 3** Temporal auto-correlation of the zonal wind stress noise averaged over the Niño34 region. For three GCMs the time correlation coefficient at a lag of one month is comparable to that in ERA-40 re-analysis data. In the ECHAM5 and MIROC models this temporal correlation is almost zero.

**Table 1** Fitted shallow water Kelvin wave speed  $c$ .

Model	$c$ [ $\text{ms}^{-1}$ ]
OBS	2.5
GFDL2.0	2.0
GFDL2.1	2.1
ECHAM5	2.0
HadCM3	1.9
MIROC	2.0

wave speed, i.e., a smaller density gradient across the thermocline, than the observed value.

### 3.4 SST equation

The response of SST to  $\tau'_x(x, y, t)$  and  $Z'_{20}$  (see Figure 1a) is described with a local linear SST anomaly equation:

$$\frac{dT'}{dt}(x, y, t) = \alpha(x, y) Z'_{20}(x, y, t - \delta) + \beta(x, y) \tau'_x(x, y, t) - \gamma(x, y) T'(x, y, t), \quad (3)$$

where  $\alpha$  is the SST response to thermocline anomalies,  $\beta$  is the direct SST response to local wind variability and  $\gamma$  is a damping term. The SST equation explains most of the variance of SST between approximately  $8^\circ\text{S}$  -  $8^\circ\text{N}$ . Outside this region values of the parameters are tapered off to very small values for  $\alpha$  and  $\beta$  and to intermediate values for  $\gamma$ . A more detailed description of the SST equation parameters is given in van Oldenborgh et al (2005) and Philip and van Oldenborgh (2008).

The two-dimensional coupling parameters used for the six versions of the ICM are fitted from ERA-40/SODA data and from the five selected GCMs. The coupling parameters

are shown in Figure 4. For observed couplings the SST variability caused by thermocline anomalies ( $\alpha$ ) is strongest in the East Pacific where the thermocline is shallowest. The response of SST to wind stress anomalies ( $\beta$ ) plays a role in SST variability in both the eastern and central Pacific. The absolute damping ( $\gamma$ ) is strongest in the east Pacific, but compared to the other terms damping is very large in the West Pacific. For more details see also Philip and van Oldenborgh (2008).

Although the GCMs were selected on having fairly realistic couplings along the equator, there are differences with the couplings derived from observations. Most models have SST variability caused by thermocline anomalies that is extended somewhat farther to the north in the East Pacific and to the west. For HadCM3 the strongest response is confined to the coast. The response simulated in the MIROC model is slightly smaller than observed. The fitted responses of SST to wind stress anomalies show only small differences. The most important differences are a weaker response in the central to western Pacific for GFDL2.1, a 10% stronger response for HadCM3 and a response for MIROC that is 20% weaker in the East Pacific and 20% stronger in the West Pacific. The modeled damping is in general about 25% weaker, with minor differences from the pattern of damping derived from reanalysis data.

## 4 Nonlinear extensions

In this study we consider two non-linear extensions to the atmospheric component discussed in the previous section: a second order term in the statistical atmosphere and the dependence of wind stress noise on the background SST (see Figure 1). Non-linearities in the ocean model are not yet considered.

### 4.1 Statistical atmosphere model

The nonlinear response of wind stress to SST is represented by the second term of a Taylor expansion in the statistical atmosphere model:

$$\tau'_x(x, y, t) = \sum_{i=1}^n A_{2,i}(x, y) T_i'(t) + \sum_{j=1}^m B_j(x, y) T_j'^2(t) + \varepsilon_2(x, y, t) \quad (4)$$

where the patterns  $A_{2,i}(x, y)$  and  $\varepsilon_2(x, y, t)$  differ only slightly from  $A_{1,i}(x, y)$  and  $\varepsilon_1(x, y, t)$  in Eq. 1. The patterns  $B_j(x, y)$  are the domain-wide wind stress patterns corresponding to the squared SST anomalies in the boxes  $j = 1, 2, \dots, m$ . As the nature of the data allows for at most three boxes, in this study we chose to match these boxes with those of the linear

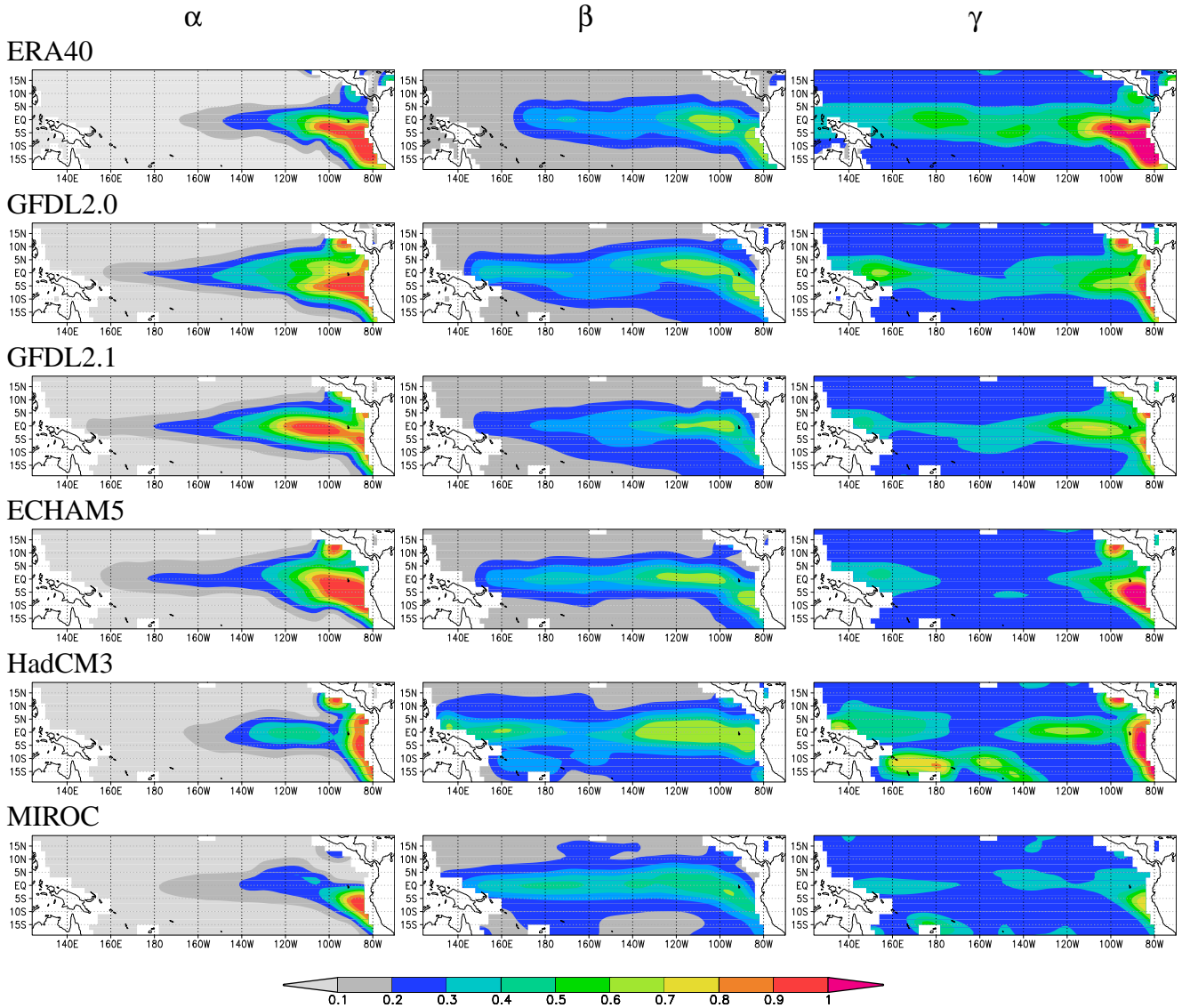


**Fig. 4** 2-dimensional parameters as described in the SST-equation (Eq. 3), for ERA-40 (top panels) and GCM output. Left:  $\alpha$ , the SST response to thermocline anomalies [ $0.1\text{Km}^{-1}\text{month}^{-1}$ ]. Center:  $\beta$ , the SST response to wind variability [ $100\text{KPa}^{-1}\text{month}^{-1}$ ]. Right:  $\gamma$ , the damping [ $\text{month}^{-1}$ ].

representation, with  $m = 3$ . Note that with the addition of the second order term in the statistical atmosphere model the first two non-zero statistical moments of the noise  $\varepsilon_2(x, y, t)$  also change slightly.

As the SST variability in the western box is small the patterns  $B_1(x, y)$  are obscured by noise. The patterns  $B_3(x, y)$  are very small compared to  $B_2(x, y)$  and therefore in Figure 5 only the nonlinear responses of wind stress to SST in the central boxes of ERA-40 and the GCMs are shown.

For ERA-40 the maximum (eastward) second order wind stress response to SST anomalies is situated just east of the mean edge of the warm pool, here defined as the  $28.5^\circ\text{C}$  isotherm. The nonlinear response shows the effect of the change in background SST. During El Niño the convection

zone is enlarged resulting in an enhanced positive response. This results in an enhancement of the westerly anomalies during El Niño. During La Niña the convection zone is reduced which leads up to reduce the negative response, again resulting in a net positive contribution (e.g., Philip and van Oldenborgh 2008). Kessler and Kleeman (1999) already showed this phenomenon of a rectified SST anomaly additional to the linear response in a much simpler model.

The negative response just north of the equator in the West Pacific shows the opposite effect. There El Niño causes a smaller eastward wind stress response as the distance to the edge of the warm pool increases. During a cold event, with the edge of the warm pool closer to that location, the westward wind stress response to SST is larger.

The GFDL2.0, GFDL2.1 and ECHAM5 models do show this effect of convective activity in the patterns. The patterns are more sensitive to the exact location of the boxes than in ERA-40. Since in these models the edge of the warm pool is too far westward, the nonlinear response of wind to SST is also farther westward. One can also recognize the fact that SSTs are more symmetric around the equator in these patterns. However, only GFDL2.1 exhibits a response with strength similar to ERA-40. For GFDL2.0 the maximum response is twice as weak and for ECHAM5 the response is even more than twice as weak. HadCM3 shows almost no positive nonlinear response. The positive response for MIROC is north of the equator. Note that GFDL2.0 and HadCM3 also show the negative responses off the equator.

#### 4.2 The relationship between noise properties and background SST

In the description of noise  $\varepsilon_1(x, y, t)$  or  $\varepsilon_2(x, y, t)$  in terms of standard deviation  $\sigma(x, y)$  and skewness  $S(x, y)$ , the noise does not depend on the background SST. A simple method for obtaining an SST dependency is to split the noise time-series into three equally likely categories where background SST conditions of the central box are warm, neutral or cold respectively. The standard deviation and skewness are then calculated for noise in each category separately.

Results for ERA-40 are shown in Figures 6 and 7 (top panels). Changes are described with respect to the neutral phase, and only significant changes are discussed. During the El Niño phase the amplitude  $\sigma(x, y)$  of the noise is up to 65% stronger in the West Pacific. During La Niña the difference in amplitude is much smaller. Contrary to what we expect, the small change indicates up to 25% larger noise amplitudes in the central to western Pacific. The skewness of the noise indicates that westerlies are spread out over a larger area just south of the equator during El Niño. The stronger noise skewness during neutral conditions than during El Niño conditions has been suggested to play a role in initiating the onset of an El Niño (Kug et al 2008b). The positive skewness during cold conditions is much lower and more confined to the West Pacific.

Differences in GCM noise are described in the light of ERA-40 results. The changes in noise amplitudes (Figure 6) of the warm phase from GFDL2.0, GFDL2.1 and ECHAM5 resemble the differences seen in ERA-40, although for GFDL2.1 the change is larger, namely 100%. Differences in the noise amplitude of HadCM3 and MIROC are much smaller. For the cold phase, GFDL2.0, GFDL2.1 and HadCM3 show a small increase in noise amplitude of about 20%, similar to observations. For GFDL2.0, GFDL2.1 and ECHAM5 westerlies indeed extend further to the east during El Niño and are more confined to the West Pacific during La Niña (Figure 7). However, the skewness is highest for warm condi-

tions in all three GCMs. The difference in skewness of HadCM3 and MIROC noise is not considered, since the noise shows no significant skewness to begin with.

## 5 The ENSO cycle

So far, all couplings and the noise shown in Figure 1 have been fitted to observations and GCMs. We compared these properties of observations with properties of the GCMs. We now want to validate the approach and check that the linear reduced models capture the main characteristics of the ENSO cycle. This is achieved by tuning our ICM using the diagnostics corresponding to each of the five GCMs or ERA-40/SODA data.

First, linear versions of the reduced model are built and examined for the ability to capture the most important ENSO properties as manifested in the original GCM or reanalysis data. Next, atmospheric nonlinearities are added in order to investigate their influence on the ENSO cycle. These nonlinearities include a realistic representation of the skewness of the noise, the nonlinear response of the statistical atmosphere and state dependent noise characteristics. For each combination of parameter settings the ICM is run for 400 years, with a spin-up time of 10 years.

Several ENSO characteristics will be discussed. These include the first EOF of SST anomalies (EOF1), the spectrum of the corresponding principal component (spectrum), the amplitude, defined by the maximum standard deviation of the SST in the East Pacific (off the coast), and the skewness of SST. The EOF1, amplitude and SST skewness have small random error margins in the ICM runs. With the decorrelation scale of SST of 6 months, errors in amplitude  $A$  and skewness  $S$  become  $0.03A$  and  $0.09$  respectively. The width of the spectra are robust, but single peaks cannot be interpreted in terms of dynamics.

Some constraints have been implemented in the ICM runs. The thermocline is forced not to outcrop above the surface. Furthermore, since the response to the western box in the nonlinear statistical atmosphere is not discernible from sampling noise, this 'signal' is included in the noise characteristics. The quadratic term of the statistical atmosphere is the only nonlinear term in the central Pacific, and in the ICMs this term is never compensated by nonlinear damping terms. Therefore we cut off the nonlinear statistical atmosphere term at an SST anomaly index of  $\pm 2K$ , which corresponds to a fairly strong El Niño/La Niña. Without this restriction the ICM results would sometimes diverge because of the fixed positions of the patterns  $A_{2,i}(x, y)$  and  $B_2(x, y)$  in the statistical atmosphere that strengthen the positive feedback. The results are not very sensitive to the cut off level. Finally, the equilibria of the different reduced models are not necessarily reached for the same mean SST. As the Gmodel is an anomaly model, we subtract the mean SST of the ICM

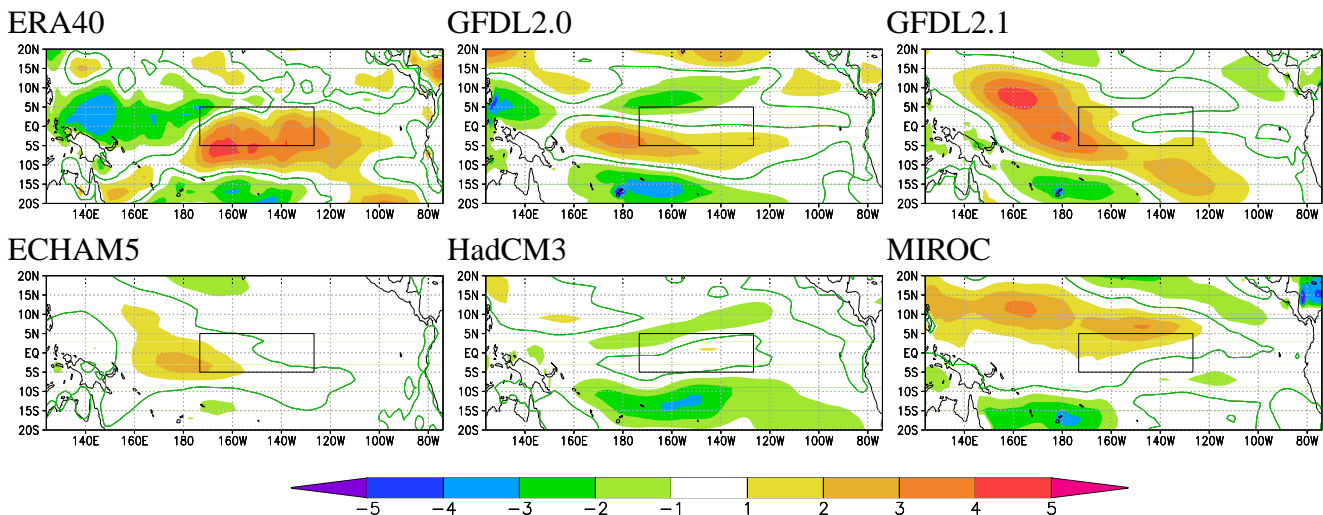


**Fig. 5** Nonlinear responses of wind stress to SST [ $10^{-3}\text{Nm}^{-2}\text{K}^{-2}$ ] in the central boxes of ERA-40 and the five GCMs. Positive numbers indicate an eastward wind anomaly. In ERA-40 and in the models that do show a positive nonlinear response near the equator, the response is close to the (modeled) edge of the warm pool.

runs to become less than 0.15 K. This did not substantially influence the ENSO characteristics.

The implementation of zonal wind stress noise generation with these prescribed standard deviation, skewness and spatial and temporal correlation lengths is described in detail in Philip and van Oldenborgh (2008).

### 5.1 The ENSO cycle in the linear reduced model

The SST anomaly equation, Kelvin wave speed, linear statistical atmosphere model and specified noise characteristics are implemented in the Gmodel framework. Without tuning any other parameters, all six fitted reduced models turn out to simulate a climate which captures the main characteristics of the ENSO cycle.

In the observations, the main factor contributing to a realistic first EOF appears to be a correct characterization of the standard deviation of the noise, with realistic spatial correlations (Philip and van Oldenborgh 2008). The skewness of the noise has only minor influence on the ENSO cycle. Therefore we now discuss only OBS-ICM experiments with noise described solely by the standard deviation, spatially and temporally correlated. A more detailed discussion of the ICM fitted to weekly ERA-40 reanalysis data can be found in Philip and van Oldenborgh (2008).

The first EOF of SST of the OBS-ICM experiment stretches about as far to the West Pacific as in the reanalysis data, and the meridional extend is smaller than in the reanalysis data (see Figure 8). The width of the spectra (at 50% of the peak value) show a large similarity, with periods between 2-7 years for ERA-40 and 1-5 years for the OBS-ICM (Fig-

ure 9). The amplitude of 0.8 K is slightly lower than the amplitude of the ERA-40 reanalysis (Table 3).

Like the OBS-ICM, the GCM-fitted ICMs are found to be relatively insensitive to the noise skewness. Therefore we made no distinction between ICM runs with and without realistically skewed noise.

Results of the EOFs for the GCM-ICMs can be found in Figure 8. The first EOFs of ICM runs of GFDL2.1, HadCM3 and MIROC are in reasonable agreement with the corresponding GCM EOFs, although the meridional extend in the MIROC-ICM is clearly too narrow. The conspicuous maximum in EOF1 in HadCM3 in the central Pacific and the far extension of EOF1 to the West Pacific in MIROC are most likely related to the strong response of SST to wind stress anomalies in the central to West Pacific. The first EOFs of GFDL2.0 and ECHAM5 in the ICM runs extend too far to the East Pacific compared to the GCMs. Spatial correlation coefficients between the GCM EOFs and the ICM EOFs are listed in Table 2.

The spectra (Figure 9) show several striking similarities between the ICMs and the GCMs. In most models the width of the spectra are almost equally broad. Note that for the ECHAM5, GFDL2.0, HadCM3 and MIROC models the width of the spectra are similar. The spectrum of the GFDL2.1 ICM is more confined than in the GCM run: 2-4 years versus 2-6 years. The overall correlation between width of the spectra of the reanalysis data and GCMs and their corresponding ICM run is 0.9.

Table 3 shows the SST amplitudes. The ECHAM5-ICM amplitude is much lower than expected, whereas the HadCM3-ICM amplitude is higher than expected. The MIROC-ICM amplitude is also very low, but this is in line with the low amplitude in the GCM. For MIROC this is most likely re-

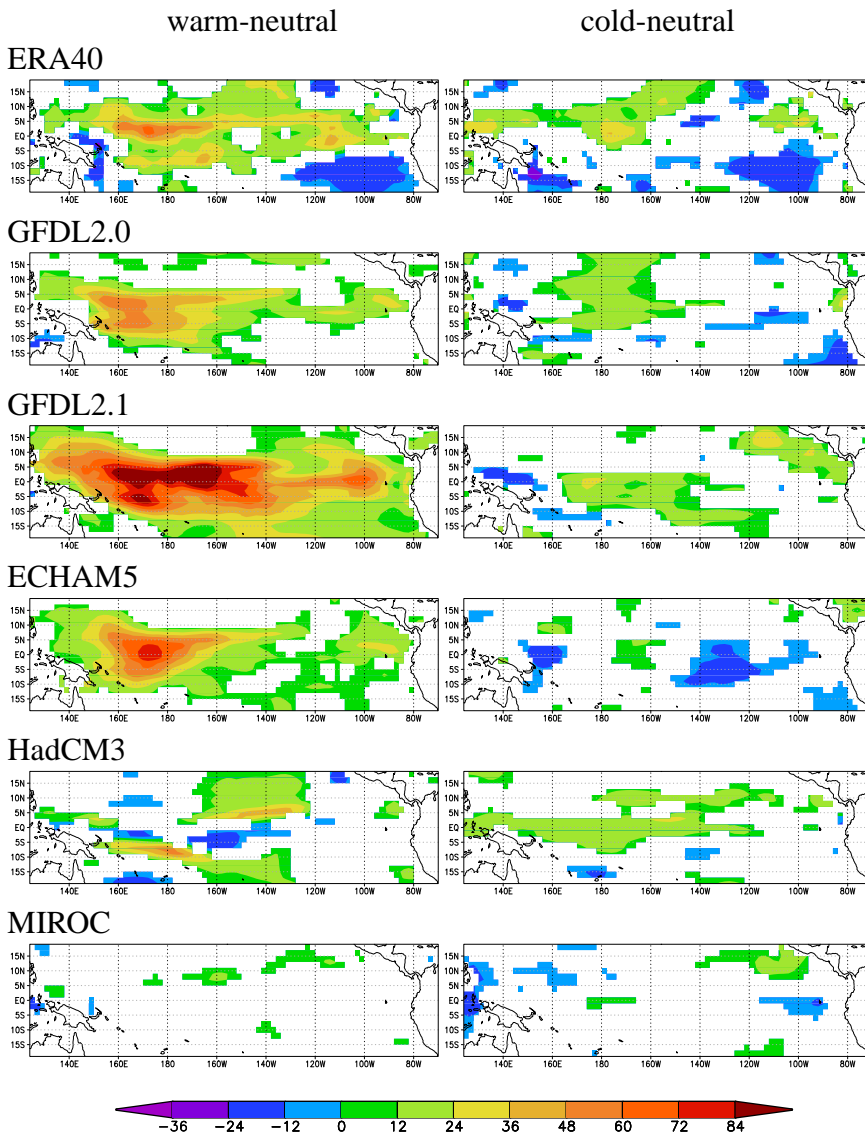


**Fig. 6** State dependent atmospheric noise standard deviation in ERA-40 and GCMs. Percentage of change in noise in the warm phase with respect to the neutral phase (left) and in the cold phase with respect to the neutral phase (right). Non-significant changes are masked out.

lated to the atmospheric noise, which has a much too low amplitude and no temporal correlation.

The Kelvin wave speed in the ICMs could be changed in order to match the ENSO amplitude in the ICM runs much better with the original ENSO amplitudes. A change in the Kelvin wave speed would also shift the peak value of the ENSO spectrum. We decided to fit the Kelvin wave speed for the best ocean dynamics and not for the best ENSO amplitude or period. With a 1.5 layer ocean model our ICM consists of only one Kelvin wave speed. It was beyond the scope of this article to study the influence of Kelvin waves corresponding to higher order vertical modes.

In general, there is a good agreement between the first EOFs and spectra of the GCMs and their corresponding ICM after fitting only linear coupling strengths. The SSTs of ICM

versions do manifest outliers like the broad power spectrum and low amplitude of MIROC SST variability and the isolated maximum of the first EOF in the central Pacific in HadCM3 SST. The extend to which the ICM SST properties agree with the GCM SST properties is model dependent. Details of SST variability in the coastal zone of South America are not simulated correctly. This is partly the result of a low model resolution and a relatively simple description of the atmosphere. Also, ocean nonlinearities are disregarded.

Overall, we conclude that the linear ICM versions reproduce the characteristics accurately enough to use them for further study: all fitted ICMs turn out to simulate the main properties of ENSO. The investigation of the influence of atmospheric properties on these model versions could improve the performance of the models.

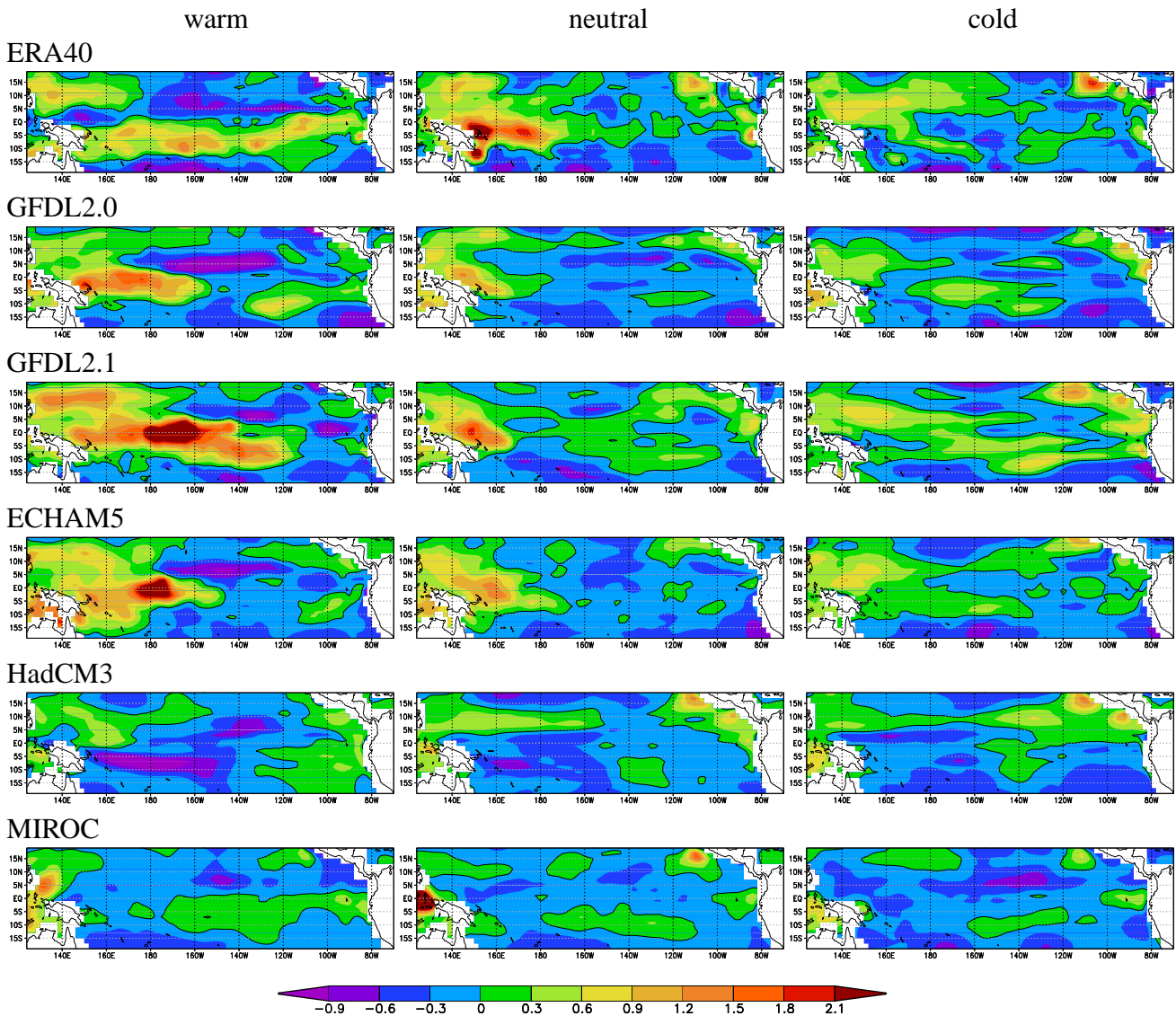


**Fig. 7** State dependent atmospheric noise skewness in ERA-40 and GCMs during the warm phase (left), the neutral phase (center) and cold phase (right). Only significant changes are mentioned in the text. The changes in HadCM3 and MIROC noise skewness are not significant.

**Table 2** Spatial correlation coefficients ( $15^{\circ}\text{S}$ :  $15^{\circ}\text{N}$ ,  $140^{\circ}\text{E}$ :  $280^{\circ}\text{E}$ ) of the first EOFs of reanalysis data and GCMs and their corresponding ICM run.

data	correlation
ERA-40	0.9
GFDL2.0	0.5
GFDL2.1	0.8
ECHAM5	0.8
HadCM3	0.7
MIROC	0.7

**Table 3** Measure for the ENSO amplitude as defined by the maximum standard deviation (sd) [K] in the East Pacific for reanalysis data and GCMs and their corresponding ICM run.

data	reanalysis/GCM	ICM
ERA-40	1.2	0.8
GFDL2.0	2.0	1.4
GFDL2.1	2.0	2.1
ECHAM5	1.9	0.6
HadCM3	1.5	2.2
MIROC	0.8	0.5

## 5.2 The influence of nonlinearities on the ENSO cycle

The second order term of the statistical atmosphere model and the relation between noise and the background SST have

been added to the linear ICM. Their influence has been investigated separately and in combination. Just like the linear model versions, all fitted ICMs turn out to simulate the main properties of ENSO. Except for the GFDL2.1-ICM spec-

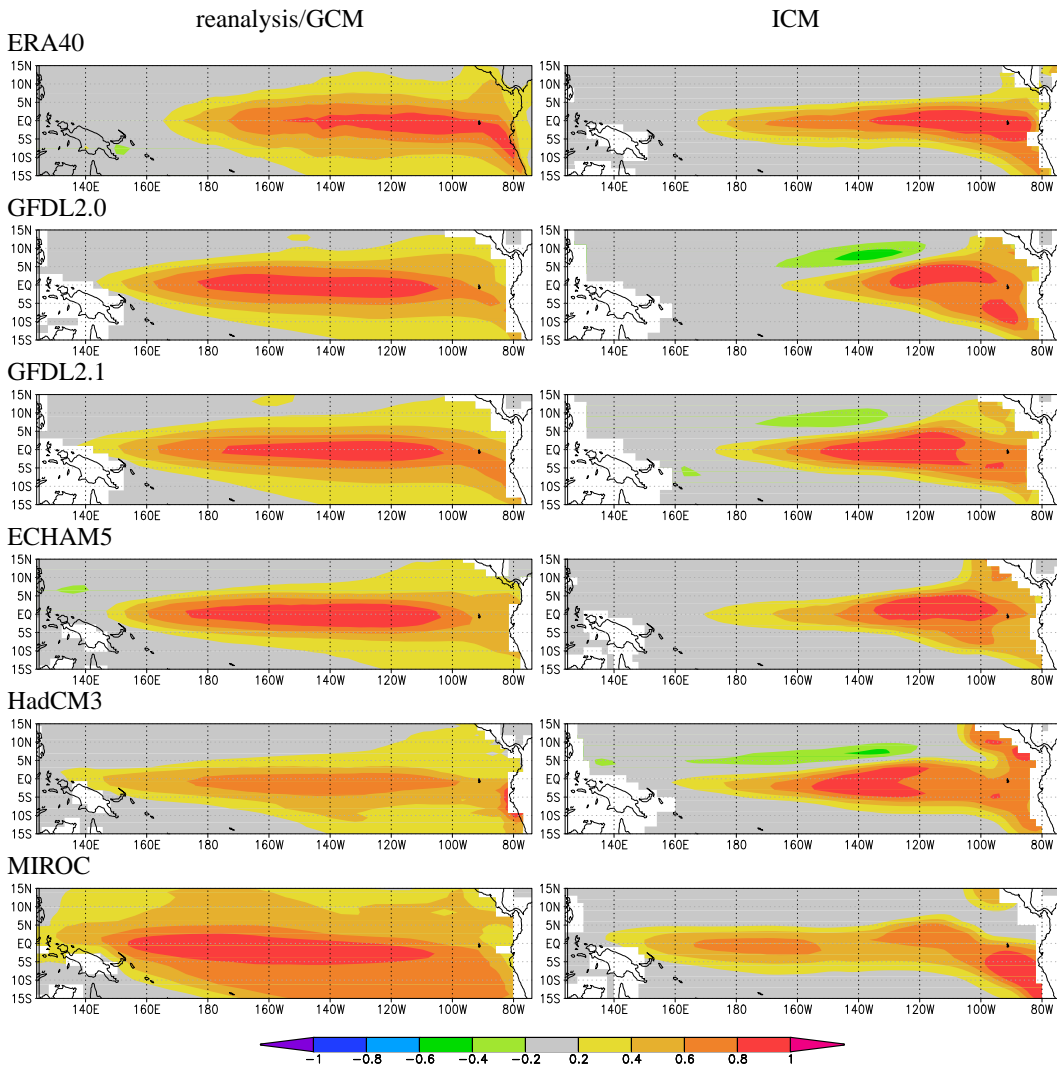


**Fig. 8** First EOF of SST anomalies of reanalysis/GCMs (left) and corresponding ICMs (right). Spatial correlation coefficients between the original and ICM EOFs are listed in Table 2.

trum (see Figure 9), the first EOFs, spectra and amplitude in all ICM runs turn out to be relatively insensitive to the modifications. Therefore in this section only the modeled SST skewness will be elaborated upon.

In the OBS experiments, the largest changes in the ICM runs are seen after adding the combination of the nonlinear response of wind stress to SST and the relation of noise to background SST. (This is in contrast to the study by Philip and van Oldenborgh (2008) in which weekly data are used. There the influence of the nonlinear statistical atmosphere has a larger influence on SST skewness than the relation of noise to the background SST.) Figure 10 shows the skewness of SST anomalies of reanalysis and GCM data, of the ICMs with a linear atmosphere ('linear ICM') and of the ICMs with both nonlinearities added ('nonlinear ICM'). The results of the ICMs in which the nonlinearities have been added separately are not shown, they are only discussed below. The focus is on the most conspicuous effects. Only

changes that are significant are mentioned in the text. Note that in the linear ICMs the SST can already be skewed due to the non-uniform mean thermocline depth; the East Pacific SSTs are most affected by the constraint that the thermocline can not outcrop above the sea surface. Relaxing this criterion gives a poorer resemblance to the observed SST skewness. Relative differences between SST skewness of the different ICM runs remains the same.

The SST output of the linear OBS-ICM run is not considerably skewed. ICM runs with skewed noise show values similar to runs where noise has zero skewness. Both the run with the dependence of noise to the background SST and the run with nonlinear wind response to SST are slightly positively skewed in the central and western Pacific with values up to 0.4, and slightly negatively skewed in the West Pacific. In the latter run the pattern shows the effect of the negative second order wind stress response to SST. The combination of the two nonlinearities is almost a linear combination, with

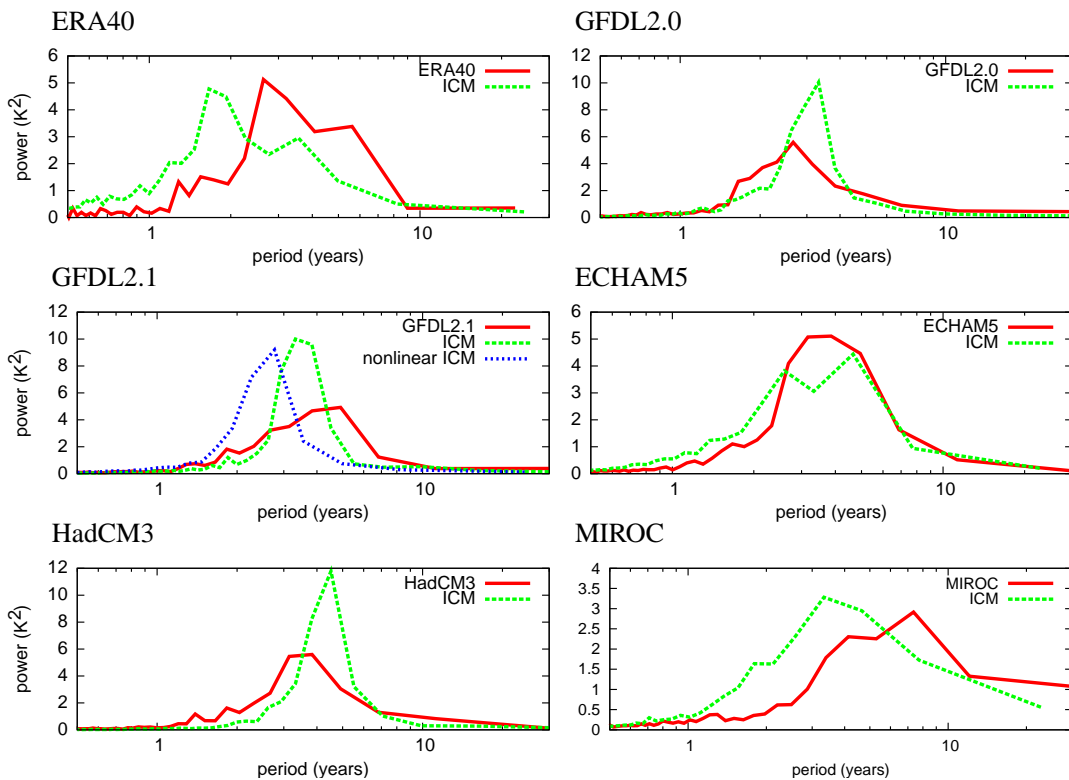


**Fig. 9** Spectra of the principal components of the first EOFs of reanalysis/GCMs and corresponding linear ICM runs. The spectra for the nonlinear ICM runs are not shown as they are not significantly different from the spectra of the linear ICM runs, except for that of GFDL2.1 with the nonlinear statistical atmosphere.

positive skewness up to 0.8. For the Niño34 timeseries this means that the ten largest warm events have a mean anomaly of 1.5 K and the ten largest cold events only reach -1.0 K.

Results for the GCMs are shown in Figure 10. As there is a large diversity of responses the experiments are discussed per model.

In the GFDL2.0-ICM the negative off-equatorial second order wind stress response to SST (Figure 5) is reflected in corresponding areas of negative skewness in both the GCM and the nonlinear ICM. The difference between the positive SST skewness of the linear GFDL2.0 ICM and the ICM with nonlinear statistical atmosphere is smaller than expected from the nonlinear response of wind stress to SST. However, differences between other GFDL2.0-ICM runs are even smaller. The positive SST skewness of 0.5 in the eastern Pacific in the ICM is only slightly lower than the GCM skewness, but the negative skewness in the West Pacific is not captured by the ICM.

For GFDL2.1 the SST skewness of the linear ICM is exceptionally high, and the pattern agrees with the GCM skewness pattern. This implies that the interaction of the thermocline with the surface is an important factor causing skewness in this model. After adding only the second order term in the statistical atmosphere the skewness is somewhat lower. This model is the only one that shows a shift in the spectrum towards shorter periods with this additional term

(indicated by the blue line in Figure 9). Using the state dependence of the noise results in a much larger SST skewness. A closer inspection of the statistical atmosphere shows that a damping term is missing in the ICM analysis, see also Section 5.3. Note that the ICM SST also shows the negative SST skewness in the West Pacific.

For the ECHAM5 SST skewness equally large influences found for the nonlinear response of wind stress to SST and the dependence of noise on the background SST. The combination of the terms gives the highest SST skewnesses, but it is relatively low compared to observations and to the original GCM. The ICM does not capture the negative skewness in the West Pacific.

The HadCM3-ICM runs display much larger SST skewnesses than the GCM SSTs. The negative skewness bands of the nonlinear atmosphere are clearly seen in both the nonlinear ICM and the GCM.

For the MIROC-ICM runs the largest differences are found after adding the nonlinear response of wind stress to SST. The off-equatorial wind stress pattern results in a small positive SST skewness in the central to western equatorial Pacific.

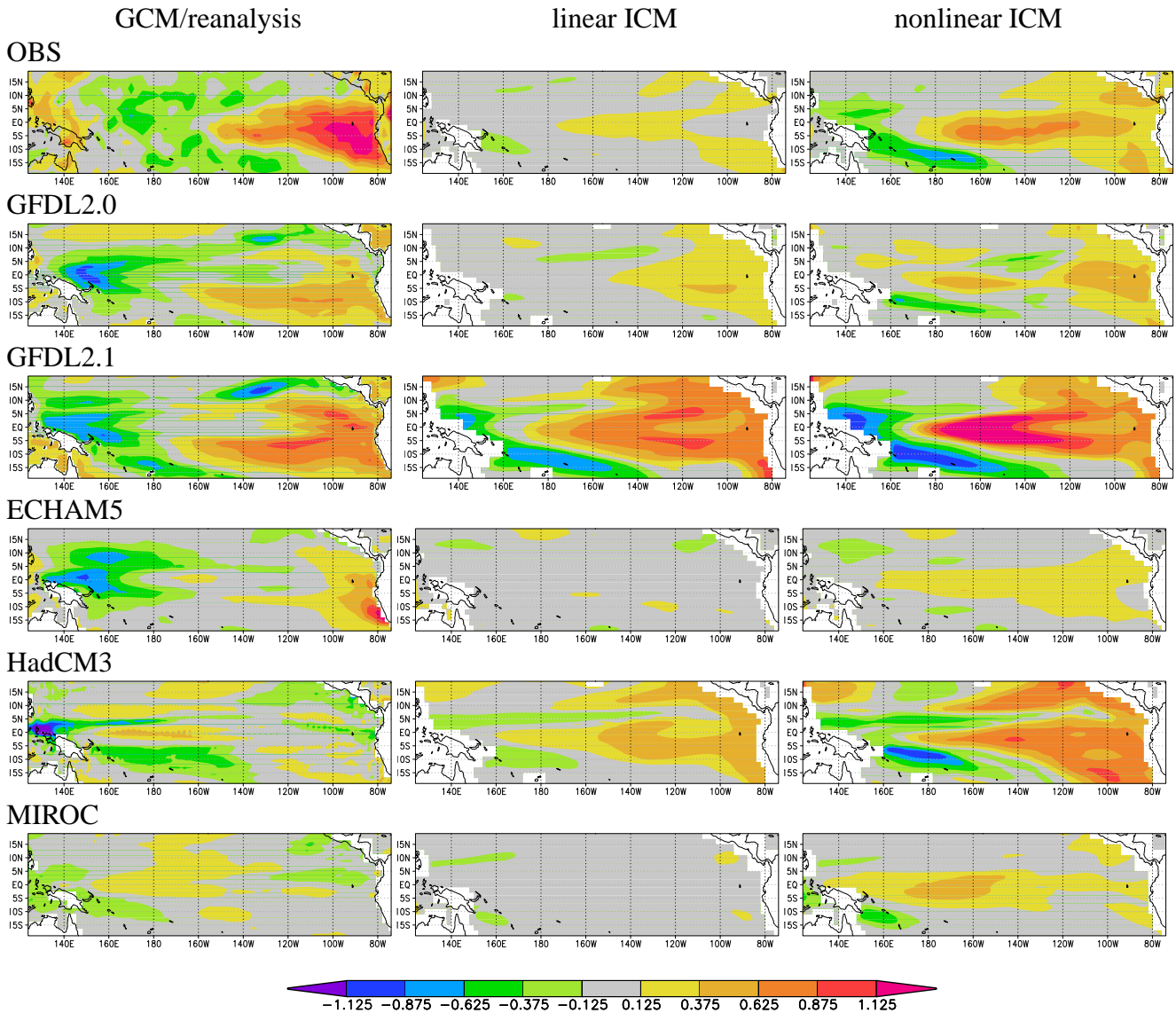


**Fig. 10** Skewness of SST anomalies of reanalysis/GCMs, linear ICM and nonlinear ICM. The thermocline is constrained not to outcrop above the sea surface. In the linear ICM the linear statistical atmosphere is used and the noise does not depend on the background SST. In the nonlinear ICM runs both the nonlinear response of wind stress to SST anomalies and the state dependence of the amplitude of atmospheric noise are added.

### 5.3 Discussion on the nonlinear extensions

In most ICM runs the region of maximum SST skewness is more towards the west than in the original GCM. While an improvement, the inclusion of atmospheric nonlinearities is only a first step towards building fully realistic reduced models. A full implementation will also have to consider nonlinearities in the ocean model. These tend to reduce the skewness in the central Pacific (Philip and van Oldenborgh 2008), and increase it in the eastern Pacific (e.g., Jin et al 2003).

The ENSO of the GFDL2.1-ICM is clearly too regular in comparison with the original GCM. Moreover, this is the only ICM in which the period changes when adding the nonlinear statistical atmosphere term. Presumably this

is due to a damping term that is missing in the ICM and one suggestion is an extra damping term in the statistical atmosphere model. When temperatures in the Niño34 region exceed  $28^{\circ}\text{C}$  in the GCM the zonal temperature gradient west of  $170^{\circ}\text{E}$  changes sign. As a result, west of  $170^{\circ}\text{E}$  the wind response to SST anomalies then reduces almost linearly, contrary to the general increase of the wind response to larger SST anomalies. The definition of the statistical atmosphere model used so far is thus no longer valid.

Both the state dependence of atmospheric noise and the second order term in the statistical atmosphere of HadCM3 are small. Nevertheless, the nonlinear statistical atmosphere significantly influences the SST skewness. This is due to the relatively large amplitude of the nonlinear wind response to

SST anomalies in the eastern box compared to the central box (not shown).

The results show that the five GCMs contain very different nonlinearities in their atmospheric components. How these relate to the model formulation could be studied systematically using a perturbed-physics ensemble such as the one described in Murphy et al (2004) and Toniazzo et al (2008).

## 6 Conclusions

This paper tries to show the most important characteristics in atmospheric properties in observations and GCMs influencing the ENSO cycle. We focus on the properties of the wind stress noise and the (nonlinear) zonal wind response to equatorial SST anomalies. The noise is defined as the wind stress residual of the statistical atmosphere model. Conclusions about this are drawn in two stages. In the first subsection we compare the strength of the couplings in the ENSO feedback loops and the properties of the noise in GCMs to reanalysis data. In the second subsection we consider the influence of the coupling strengths and noise on the ENSO cycle.

### 6.1 Direct comparison of GCMs with observations

For a selection of five GCMs with the most realistic main ENSO feedbacks, noise terms and the dependence of noise on the background SST have been characterized and compared to the ERA-40 reanalysis. Subsequently, the nonlinear response of zonal wind stress to SST anomalies has been characterized.

The amplitude of zonal wind stress noise near the equator (i.e. wind stress anomalies unrelated to equatorial SST) is in general lower in GCMs than in the ERA-40 reanalysis. The difference ranges between 20% lower (GFDL2.1) to 200% lower (MIROC). Furthermore, the lagged autocorrelation of the monthly noise fields near the equator is almost zero in the ECHAM5 and MIROC models, in contrast to the observed value of 0.4 at lag one month. However, the pattern of lowest standard deviation in the equatorial East Pacific and higher in the equatorial West Pacific is captured. Also, spatial correlation lengths of noise fields are comparable to observed values. So, models need stronger, coherent subseasonal variability (see also e.g. Slingo et al 1996; Lin et al 2006).

Low standard deviations and temporal correlations of the wind stress noise influence the ENSO amplitude. Comparing the GCMs to each other, the MIROC model has indeed by far the lowest ENSO amplitude. As the other coupling strengths of the ENSO cycle deviate less from observations, the low variability and temporal coherence of the westerly

wind in the western and central Pacific seem the most important factors explaining the low ENSO amplitude in this model.

SST skewness is influenced by two other characteristics of the noise fields. First, the skewness of the noise fields of reanalysis data is characterized by a positive values in the West Pacific (stronger westerly anomalies than easterly anomalies). Only three GCMs show comparable noise skewnesses. Second, the noise depends on the background state. In reanalysis data the noise amplitude is larger when SST anomalies are positive than during neutral SST conditions and the positive skewness extends further to the east. The GCMs do simulate this dependence of noise on the background SST, but only the GFDL2.0, GFDL2.1 and ECHAM5 models show differences of comparable size.

Reanalysis data indicate that SST anomalies in the central Pacific result in an eastward second order wind stress response near the edge of the warm pool. In the GFDL2.0, GFDL2.1 and ECHAM5 models we find a similar response, with maxima at locations corresponding to the edges of the modeled warm pools. HadCM3 shows no indications for an eastward nonlinear response for both El Niño and La Niña, and in MIROC the eastward response is only north of the equator. Off-equatorial bands of westward wind stress responses to SST anomalies in the central Pacific are seen in reanalysis data. GFDL2.0, HadCM3 and to a lesser extend also GFDL2.1 and MIROC show similar off-equatorial bands.

Previous findings stressed the importance of the nonlinear atmospheric response to the skewness of SST. Indeed, the simplified models that represent this response most realistically also have the most realistic SST skewness. Results from the GFDL2.1 model show a nonlinear response to SST with strength roughly equal to the strength in the reanalysis data. In the same model, the SST skewness pattern resembles the observed SST skewness pattern quite well. The nonlinear responses of GFDL2.0 and ECHAM5 wind stress to SST are weaker, and so is their calculated SST skewness. The wind stress patterns of HadCM3 and MIROC are very different from the patterns in reanalysis data, and these GCMs do not simulate the observed SST skewness at all. The nonlinear response of wind stress to SST is therefore thought to be directly related to SST skewness.

Overall, the standard deviation and time-correlation of the noise are in general underestimated. Three models simulate noise skewness and the dependence of noise on the background SST with strengths comparable to those in ERA-40 reanalysis data. The three models with the most realistic nonlinear response of wind stress to SST appear to simulate the best SST skewness.

## 6.2 Comparison of the ENSO cycle in GCMs with observations using reduced models

To study the impact of the coupling strengths and noise properties on the ENSO cycle, the fitted parameters are used to make six versions of an ICM, corresponding to the observations and the five GCMs under study. These reduced models can simulate the main properties of ENSO in observations and GCMs. The first step includes the direct feedbacks and noise characteristics. Later, the nonlinear response of wind stress to SST and the relation of noise to the background SST are added to these linear ICM versions.

Analyses of the SST output of the linear ICMs show that the first EOFs are approximated reasonably well. The width of the spectra of the corresponding principal components are reproduced well by the reduced models, although the position of the peak is sometimes shifted. These ENSO properties do not change significantly after adding either the nonlinear response of wind stress to SST or the relation of noise to the background SST.

The observed ENSO amplitude is slightly stronger than in the runs of the ICM fitted to observations. The GCM and corresponding ICM amplitudes are correlated, although the correspondence is not perfect. In the MIROC model low noise standard deviations and temporal correlation can indeed be seen in the corresponding ICM run. The ECHAM5 model is an exception: it is yet unexplained why modeled ENSO amplitude in the GCM is three times higher than in the ICM. One factor that influences the correspondence between GCM and ICM ENSO amplitudes is the Kelvin wave speed. The Kelvin wave speed is fitted for the best ocean dynamics and not for the best ENSO amplitude. Other possible factors influencing the ENSO amplitude have not yet been investigated in detail.

The ICMs reproduce the skewness in the reanalysis and GCMs fairly well. However, the skewness maps are in general not exactly the same, as the feedbacks characterized so far in the ICMs do not represent the full complexity of the system.

The ICM SST skewness is influenced by both the nonlinear response of wind stress to SST and the dependence of noise on the background SST. For monthly reanalysis data the impacts of both nonlinearities are about equally large and are nearly additive. In the GCMs the relative strengths of these two nonlinearities differ.

The wind stress noise itself is also nonlinear: westerly wind anomalies are larger than easterly ones. However, this has only a minor influence on SST skewness in the ICM experiments.

Overall, we have built reduced models with linear feedbacks, atmospheric noise terms and a nonlinear response of wind stress to SST fitted to observations and GCMs. The linear ICMs capture ENSO characteristics like the first EOF

and spectrum of the corresponding time series quite well. In both observations and GCMs, the influence of the skewness of noise has a smaller influence on the ENSO cycle than the standard deviation of the noise. For monthly observations both the nonlinear response of wind stress to SST anomalies and the relation of noise to the background SST contribute to SST skewness. GCMs that simulate a nonlinear response of wind stress to SST anomalies in general agree on this, although the relation of noise to the background SST is relatively more important in the climate models.

With this analysis a step forward has been made in building a realistic reduced model that describes the observations and GCMs in the equatorial Pacific region. There are still terms to be added in order to refine the ICMs. Further investigation per model is needed in order to refine the results. This will result in better understanding of the dynamics and in improvements in models and model predictions.

**Acknowledgements** We acknowledge the international modeling groups for providing their data for analysis, the PCMDI for collecting and archiving the model data, the JSC/CLIVAR Working Group on Coupled Modelling and their Coupled Model Intercomparison Project and Climate Simulation Panel for organizing the model data analysis activity, and the IPCC WG1 TSU for technical support. We kindly thank Matthew Collins and Bart van den Hurk for comments and suggestions. This research is supported by the Research Council for Earth and Life Sciences (ALW) of the Netherlands Organisation for Scientific Research (NWO).

## References

- An SI, Hsieh WW, Jin FF (2005) A nonlinear analysis of the ENSO cycle and its interdecadal changes. *J Climate* 18:3229–3239
- Blanke B, Neelin JD, Gutzler D (1997) Estimating the effect of stochastic wind stress forcing on ENSO irregularity. *J Climate* 10:1473–1486
- Burgers G, Balmaseda MA, Vossepoel FC, van Oldenborgh GJ, van Leeuwen PJ (2002) Balanced ocean-data assimilation near the equator. *J Phys Oceanogr* 32:2509–2529
- Burgers GJH, van Oldenborgh GJ (2003) On the impact of local feedbacks in the Central Pacific on the ENSO cycle. *J Climate* 16:2396–2407
- Carton JA, Giese BS (2008) SODA: A reanalysis of ocean climate. *MWR* 139:2999–3017
- Eisenman I, Yu L, Tziperman E (2005) Westerly wind bursts: ENSO's tail rather than the dog? *J Climate* 18:5224–5238
- Gebbie G, Eisenman I, Wittenberg A, Tziperman E (2007) Westerly wind burst modulation by sea surface temperature as an intrinsic part of ENSO dynamics. *J Atmos Sci* 64:3281–3295
- Gill AE (1980) Some simple solutions for heat induced tropical circulation. *Quart J Roy Meteor Soc* 106:447–462
- Gill AE (1982) *Atmosphere–Ocean Dynamics*. Academic Press, Orlando, 662 pp.
- Guilyardi E (2006) El Niño - mean state - seasonal cycle interactions in a multi-model ensemble. *Climate Dyn* 26:329–348
- Jin FF, An SI, Timmermann A, Zhao J (2003) Strong El Niño events and nonlinear dynamical heating. *Geophys Res Lett* 30(3):1120, DOI 10.1029/2002GL016356
- Kessler W, Kleeman R (1999) Rectification of the Madden-Julian oscillation into the ENSO cycle. *J Climate* 13:3560–3575

- Kleeman R, Moore A, Smith NR (1995) Assimilation of subsurface thermal data into a simple ocean model for the initialization of an intermediate tropical coupled ocean–atmosphere forecast model. *Mon Wea Rev* 123:3103–3114
- Kug JS, Jin FF, Sooray KP, Kang IS (2008a) State-dependent atmospheric noise associated with ENSO. *Geophys Res Lett* 35:L05,701, DOI 10.1029/2007GL032017
- Kug JS, Sooray KP, Kim D, Kang IS, Jin FF, Takayabu YN, Kimoto M (2008b) Simulation of state-dependent high-frequency atmospheric variability associated with ENSO. *Climate Dyn* DOI 10.1007/s00382-008-0434-2, in press
- Lengaigne M, Boulanger JP, Menkes C, Madec G, Delecluse P, Guilyardi E, Slingo J (2003) The march 1997 westerly wind event and the onset of the 1997/98 El Niño: Understanding the role of the atmospheric response. *J Climate* 16:3330–3343
- Lengaigne M, Guilyardi E, Boulanger JP, Menkes C, Delecluse P, Inness P, Cole J, Slingo J (2004) Triggering of El Niño by westerly wind events in a coupled general circulation model. *Climate Dyn* 23:601–620
- Lin JLGK, Mapes B, Weickmann K, Sperber K, Lin W, Wheeler M, Schubert S, Genio AD, Donner L, Emori S, Gueremy JF, Hourdin F, Rasch P, Roeckner E, Scinocca J (2006) Tropical intraseasonal variability in 14 IPCC AR4 climate models. part i: Convective signals. *J Climate* 19:2665–2690, DOI 10.1175/JCLI3735.1
- Murphy JM, Sexton DMH, Barnett DN, Jones GS, Webb MJ, Collins M, Stainforth DA (2004) Quantification of modelling uncertainties in a large ensemble of climate change simulations. *Nature* 430:768–772
- van Oldenborgh GJ, Philip SY, Collins M (2005) El Niño in a changing climate: a multi-model study. *Ocean Science* 1:81–95
- Perez CL, Moore AM, Zavala-Garay J, Kleeman R (2005) A comparison of the influence of additive and multiplicative stochastic forcing on a coupled model of ENSO. *J Climate* 18:5066–5085
- Philander SG (1990) *El Niño, La Niña and the Southern Oscillation*. Academic Press, San Diego, 293 pp.
- Philip SY, van Oldenborgh GJ (2008) Significant atmospheric nonlinearities in the ENSO cycle. *J Climate* Submitted
- Slingo JM, Sperber K, Boyle J, Ceron JP, Dix M, Dugas B, Ebisuzakiand W, Fyfe J, Gregory D, Gueremy JF, Hack J, Harzallah A, Inness P, Kitoh A, Lau WM, McAvaney B, Madden R, Matthews A, Palmer T, Park CK, Randall D, Renno N (1996) Intraseasonal oscillations in 15 atmospheric GCMs: results from an AMIP diagnostic subproject. *Climate Dyn* 12:325–357, DOI 10.1007/s003820050112
- Toniazzo T, Collins M, Brown J (2008) The variation of ENSO characteristics associated with atmospheric parameter perturbations in a coupled model. *Climate Dyn* 30:643–656
- Tziperman E, Yu L (2007) Quantifying the dependence of westerly wind bursts on the large scale tropical Pacific SST. *J Climate* 20:2760–2768
- Uppala SM, Kålberg PW, Simmons AJ, Andrae U, da Costa Bechtold V, Fiorino M, Gibson JK, Haseler J, Hernandez A, Kelly GA, Li X, Onogi K, Saarinen S, Sokka N, Allan RP, Anderson E, Arpe K, Balmaseda MA, Beljaars ACM, van den Berg L, Bidlot J, Borman N, Caires S, Dethof A, Dragosavac M, Fisher M, Fuentes M, Hagemann S, Hólm E, Hoskins BJ, Isaksen L, Janssen PAEM, Jenne R, McNally AP, Mahfouf JF, Mcrette JJ, Rayner NA, Saunders RW, Simon P, Sterl A, Trenberth KE, Untch A, Vasiljevic D, Viterbo P, Woollen J (2005) The ERA-40 re-analysis. *Quart J Roy Meteor Soc* 130:2961–3012, DOI 10.1256/qj.04.176
- Vecchi GA, Wittenberg AT, Rosati A (2006) Reassessing the role of stochastic forcing in the 1997–1998 El Niño. *Geophys Res Lett* 33, DOI 10.1029/2005GL024738
- Von Storch H, Zwiers F (2001) *Statistical Analysis in Climate Research*. Cambridge University Press, The Edinburgh Building, Cambridge CB2 2RU, UK, ISBN 0 521 45071 3 / 0 521 01230
- Zavala-Garay J, Moore AM, Perez CL, Kleeman R (2003) The response of a coupled model of ENSO to observed estimates of stochastic forcing. *JCL* 18:2441–2459
- Zebiak SE, Cane MA (1987) A model of El Niño–Southern Oscillation. *Mon Wea Rev* 115:2262–2278
- Zhang RH, Busalacchi AJ, DeWitt DG (2008) The roles of atmospheric stochastic forcing (SF) and oceanic entrainment temperature (Te) in decadal modulation of ENSO. *J Climate* 21:674–704, DOI 10.1175/2007JCLI1665.1